RSC Advances

This is an *Accepted Manuscript*, which has been through the Royal Society of Chemistry peer review process and has been accepted for publication.

Accepted Manuscripts are published online shortly after acceptance, before technical editing, formatting and proof reading. Using this free service, authors can make their results available to the community, in citable form, before we publish the edited article. This *Accepted Manuscript* will be replaced by the edited, formatted and paginated article as soon as this is available.

You can find more information about *Accepted Manuscripts* in the Information for Authors.

Please note that technical editing may introduce minor changes to the text and/or graphics, which may alter content. The journal's standard Terms & Conditions and the Ethical guidelines still apply. In no event shall the Royal Society of Chemistry be held responsible for any errors or omissions in this *Accepted Manuscript* or any consequences arising from the use of any information it contains.

ROYAL SOCIETY OF CHEMISTRY

www.rsc.org/advances

Journal Name

RSCPublishing

ARTICLE

Facile synthesis of cerium oxide nanostructures for rechargeable lithium battery electrode materials

Cite this: DOI: 10.1039/x0xx00000x

Huan Pang* [a, b, c] and Changyun Chen,*[b]

Received 00th January 2012,
Accepted 00th January 2012

DOI: 10.1039/x0xx00000x

www.rsc.org/

A facile method is developed to synthesize cerium oxides with plate and brick morphologies by the thermal decomposition of nanostructured oxalate precursors. The electrochemical test of the Li-ion battery reveals that the as-synthesized CeO_2 nanostructures affect their electrochemical properties. Especially, the specific capacity of brick-like CeO_2 nanostructured electrode is above 460 mAh g^{-1}, and good stability up to 100 charge–discharge cycles.

Introduction

The conspicuous physical–chemical properties of nanostructures, as we all know, are sensitively correlated to their surface morphologies. It is very important to control the synthesis of nanomaterials to provide different shapes for morphology–property investigations. [1–5] Over the past two decades, the development of many chemical control syntheses of micro/nanostructured materials has been expanded from monodispersed particles to nanowires, nanorods, cables, tubes, and polygons. [6–12]

Rechargeable lithium ion batteries are the state-of-the-art power sources for portable electronic devices such as wireless phones, laptop computers and camcorders due to their high energy density and long cycle life. They have also been considered as the technology of choice for the development of hybrid electric and electric vehicles (HEVs and EVs). [13–15] The voltage, capacity, rate capability and cycle life depend on reversible extractions and insertions of lithium ions in the electrode materials during charge and discharge cycles. In the past years, large numbers of efforts have been spent on nanostructured materials to develop such clean energy storage devices by improving the performance of supercapacitors and lithium-ion batteries. [16–22]

As one of the most attractive rare earth oxides, cerium oxides (CeO_2) is an important rare earth compound which offers manifold interesting properties including oxygen storage capacity, high thermal stability, optical properties, electrical conductivity and diffusivity. [23-35] Ceria is expected to show applications as electrode materials in lithium ion battery due to the direct and fast transformation of Ce (III) and Ce (IV). Oxalates are not only obtained easily and low cost, but also have good structure stability and relatively low decomposition temperature in air. To the best of our knowledge, CeO_2 are often obtained by the calcination of the oxalate precursor at high temperature in the conventional approach. [36-39] Due to cerium oxalate salts could precipitate rapidly at room temperature, it may be difficult to control the morphology of the cerium oxalate precursor, even that of CeO_2 correspondingly. There are few reports on the fabrication of satisfied structured CeO_2 via cerium oxalate precursor in a mild synthesis route. [40]

In previous work, we have successfully synthesized some nanomaterials from nanostructured oxalate precursors, such as: mesoporous $Ni_{0.3}Co_{2.7}O_4$ hierarchical structures, [12] porous ZnO-NiO nanostructures, [41] and porous $NiMn_2O_4$ nanostructures. [42] Herein, we have successfully used nanostructured ceria oxalates as the precursors to generate nanostructured CeO_2 under a mild condition. More importantly, these CeO_2 nanostructures were successfully applied as lithium ion battery electrode materials. Interestingly, the electrodes containing brick-like particles exhibit an electrochemical capacity of ~460 mA h g^{-1}, and good stability up to 100 charge–discharge cycles.

Experimental section

Synthesis procedures

For precursors, in a typical synthesis, firstly, 0.10 g $H_2C_2O_4$, 0.10 g $Na_2C_2O_4$, 20.0 mL glycerin and 20.0 mL H_2O were mixed up and stirred for an hour, and then 0.16 g cerous nitrate were added into the solution. After being stirred, for 11 hours, we can obtain white precipitation (the plate-like precursor). The other brick-like precursor can be easily obtained by using the same amount of glycol instead of glycerin; for CeO_2 nanostructures. Two precursors were calcined in the air at 450 ^oC for 1.0 h, and the heating-up rate was 1 °C per min for the calcination. Then the straw yellow powders can be obtained.

Characterizations

The phase of these obtained samples were characterized by X-ray diffraction (XRD) on a Shimadzu XRD-6000 powder X-ray diffractometer with Cu K_α radiation (λ=1.5418 Å). The morphologies of the samples were taken by a Hitachi S-4800 field-emission scanning electron microscope (FE-SEM) at an acceleration voltage of 10.0 KV. Transmission electron microscopy (TEM) and high resolution TEM (HRTEM) images were captured on a JEOL JEM-2100 microscope at an acceleration voltage of 200 kV. Nitrogen adsorption–desorption

RSC Advances Accepted Manuscript

measurements were performed on a Gemini VII 2390 Analyzer at 77 K. Thermogravimetric analysis (TGA) was carried out in air up to 800 °C using a NETZSCH STA 409 PC instrument with a heating rate of 5 °C min^{-1}.

Preparation of lithium ion battery electrodes

The active materials were fabricated by mixing CeO_2 nanopowders, acetylene black, and PVDF at a weight ratio of 80:15:5, respectively, using N-methylpyrrolidone (NMP) as a solvent. The resulting slurries were cast onto copper current collectors, and then dried at 120 °C under vacuum for 12 h. The electrode foils were pressed at a pressure of 8.27×10^6 Pa, and then cut into disks 13 mm in diameter. CR2016 coin-type cells were assembled in an argon-filled glove box (M-braun MB20G) by stacking a microporous polypropylene separator (Celgard 2400) containing a liquid electrolyte of $LiClO_4$ (1.0 M) in ethylene carbonate (EC)/dimethyl carbonate (DMC) (1:1, v/v) between the anode and the lithium metal foil.

The batteries were tested on Land CT2001A. The cyclic voltammogram (CV) were performed on an electrochemical station-CHI 660d. Electrochemical impedance spectroscopy (EIS) measurements of all the samples were conducted at open circuit voltage in the frequency range of 100 kHz to 0.01 Hz with AC voltage amplitude of 5 mV using PARSTAT2273.

Results and discussion

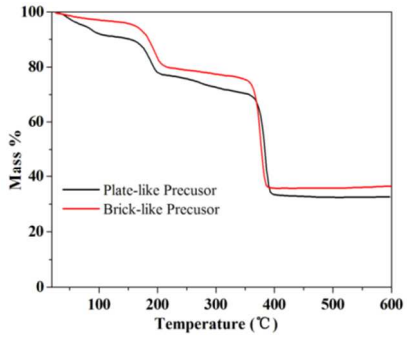

Figure 1 TG curves of two precursors.

The CeO_2 nanostructures were obtained by a precipitation method without any surfactant followed by a calcination treatment in air. Firstly, 0.1 g $H_2C_2O_4$, 0.1 g $Na_2C_2O_4$, 20 mL glycerin and 20 mL H_2O were mixed up and stirred for an hour, and then 0.16 g cerous nitrate were added into the solution. After being stirred for 11 hours, we can obtain white precipitation (the plate-like precursor). The other brick-like precursor can be easily obtained by using the same amount of glycol instead of glycerin. TG curves of precursors are shown in Figure 1, from which it is seen that the precursors have two weight loss steps and end at 400 ◦C. The precursors were calcined in the air at 450 °C for 1 h, and the straw yellow powders can be obtained.

The Powder X-ray diffraction (XRD) patterns (Figure 2) of all samples have identical peaks, and all the peaks of two precursors in Figure 2a, b can be indexed to the same phase. In Figure 2c, d, all peaks can be perfectly indexed to that of CeO_2 (Joint Committee on Powder Diffraction Standards (JCPDS) card No. 42-1467). No impurities, such as precursor compounds, can be detected, indicating the complete formation of pure cerium oxides. More importantly, we also can find that the peaks of CeO_2 are wide, which means the size of these CeO_2 particles is in nanoscale. The morphology of the precursor is shown in Figure 2e, f. Clearly, the plate-like morphology is seen in Figure 2e, and the particle size is about 8 μm. Moreover, the brick-like morphology is seen in Figure 2f, and the particle size is about 2 μm.

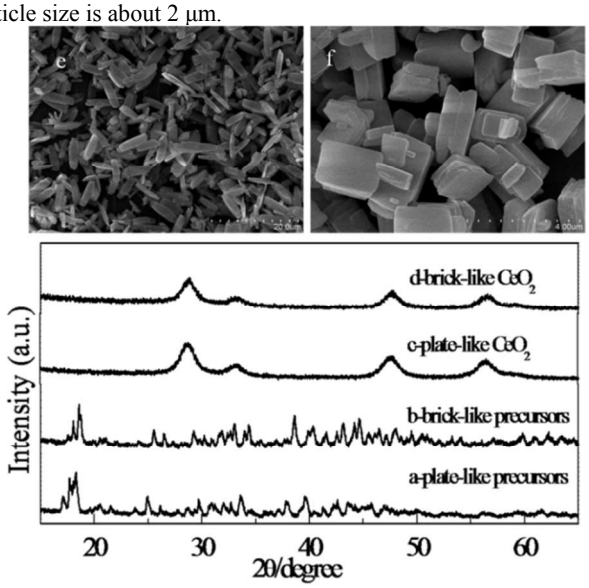

Figure 2 a-d) Powder X-ray diffraction (XRD) patterns of all samples; e-f) SEM images of the precursors.

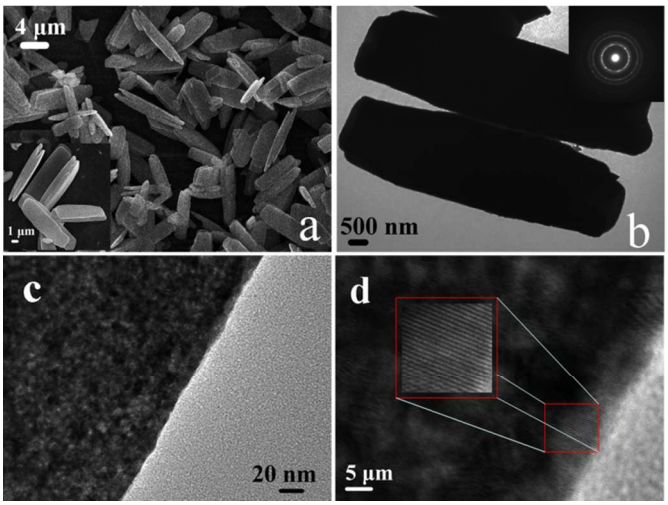

Figure 3 a) An SEM image of the plate-like CeO_2 particles; b, c) TEM images; in inset of b the corresponding selected area electron diffraction (SAED); d) The high resolution TEM (HRTEM) image of plate-like CeO_2 particles.

We have successfully synthesized two kinds of CeO_2 nanostructures after the calcination of the precursors in the air. Field-emission scanning electron microscopy (FESEM) and transmission electron microscopy (TEM) images provide insight into the morphology of the CeO_2 nanostructures. Figure 3 shows the general morphology of CeO_2 plate-like was synthesized in this work. The uniform plates are with the length of about 8 μm and thickness of about 1.5 μm (in inset of Figure 3a). From Figure 3b, TEM images shows the same size as that of FESEM image in Figure 3a, the inset

RSC Advances Accepted Manuscript

This journal is © The Royal Society of Chemistry 2012

of which is the corresponding selected area electron diffraction (SAED), and we can see the CeO_2 plate-like is made up of a plenty of CeO_2 nanocrystals. A number of CeO_2 particles accumulate the plate-like structure. From Figure 3c there are few gaps or porous structures on plate-like structure. What' more, from Figure 3d, the crystallize CeO_2 nanocrystal is evidenced from the high resolution TEM (HRTEM) image of CeO_2 plate-like particles.

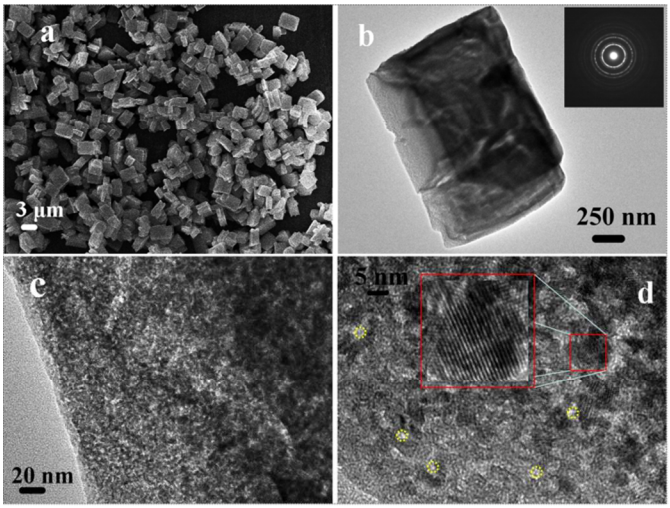

Figure 4 a) An SEM image of the brick-like CeO_2 particles; b-c) TEM images; in inset of b the corresponding selected area electron diffraction (SAED); d) An HRTEM image of brick-like CeO_2 particles.

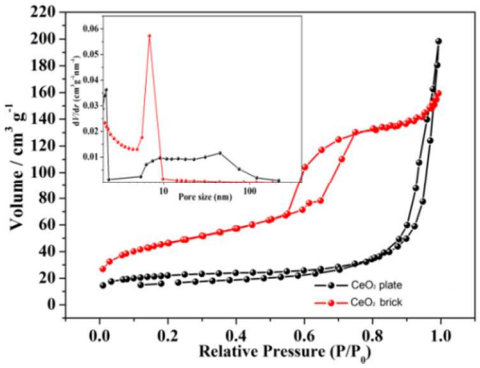

Figure 5 Brunauer–Emmett–Teller measurements of CeO_2 nanostructures; and corresponding Barrett–Joyner–Halenda pore size distribution curve in inset of it.

From the images of Figure 4, we can see that the uniform brick structures with length of about 2 μm. The SAED pattern (top inset in Figure 4b) of fringe individual brick structure indicates the polycrystalline character of the CeO_2 particles. Unlike CeO_2 plate-like particles (Figure 3c), there are several nanopores on the brick-like structure CeO_2 particles. Moreover, a HRTEM image of the brick-like structure CeO_2 particles reveals the crystalline nature of nanoparticle in inset of Figure 4d.

To gain further insight of the porous information and size distribution of as-prepared samples, BET measurements were performed (Figure 5). The brick-like structure CeO_2 particles show a distinct hysteresis in the larger range ca. 0.55–0.75 P/P_0 in Figure 5, indicating the presence of mesopores possibly formed by porous stacking of component nanoparticles. [43, 44] The BET surface area of the brick-like structure CeO_2 particles (66.7 m^2 g^{-1}) makes an efficient contact of the porous structures with the electrolyte. But that of the plate-like structure CeO_2 particles is not. The corresponding Barrett–Joyner–Halenda (BJH) pore size distribution curve in inset of Figure 5 shows that the pore size of brick-like structure CeO_2 particles is uniform, within the range of the mesopores (3~5 nm), while that of plate-like structure CeO_2 particles does not have. These porous structures of brick-like structure CeO_2 particles do not only offer enough surface areas, but provide electrolyte accesses. The morphology of brick might offer a stable structure for Li ion intercalated/extracted into/out, which might improve the electron transfers and cycle life of the electrode. [45–49]

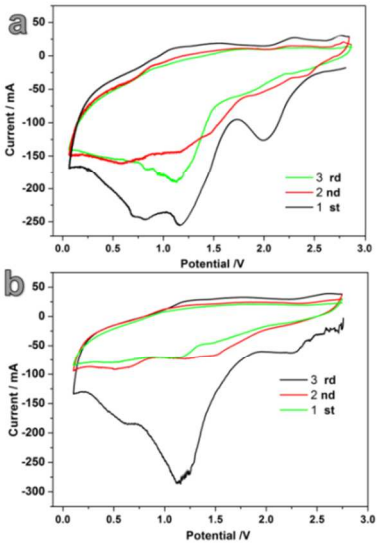

Figure 6 CV curves of electrodes for 1st, 2nd and 3rd cycles at a scan rate of 0.1 mV s^{-1}, a) plate-like CeO_2 particles, b) brick-like CeO_2 particles.

Cyclic voltammetry (CV) measurements were conducted to evaluate the Li storage performance of the CeO_2 nanostructures in Figure 6. The CV curves were tested at a scan rate of 0.1 mV s^{-1} in the potential window of 0.02–2.75 V versus Li. As shown in Figure 6, two reduction peaks located at 0.6 and 1.2 V are detected in the first cathodic scan, which can be assigned to the initial reduction of CeO_2 to Ce ($CeO_2 + 4Li^+ + 4e^- = Ce + 2Li_2O$) and the formation of amorphous Li_2O and solid electrolyte interphase (SEI).[50-53]The oxidation peak is observed at 2.58 V in the anodic scan, corresponding to the CeO_2 formation and Li_2O decomposition ($Ce + 2Li_2O = CeO_2 + 4Li^+ + 4e^-$, the theoretical specific capacity of CeO_2 is 623 $mAhg^{-1}$). The reduction and oxidation peaks respectively shift for the subsequent cycles due to the drastic lithium driven, structural or textural modifications.[53, 54] In the cathodic polarization process of the first cycle, the redox peak of the CeO_2 nanostructured electrodes appears at different voltages. However, during the second and third cycles, the redox peak of the CeO_2 nanostructured electrodes appears nearly at the same voltages albeit with low peak intensity respectively. Therefore, it also suggests the lithium insertion and deinsertion processes and the formation of amorphous Li_2O and SEI. [55]

RSC Advances Accepted Manuscript

Journal Name

RSCPublishing

ARTICLE

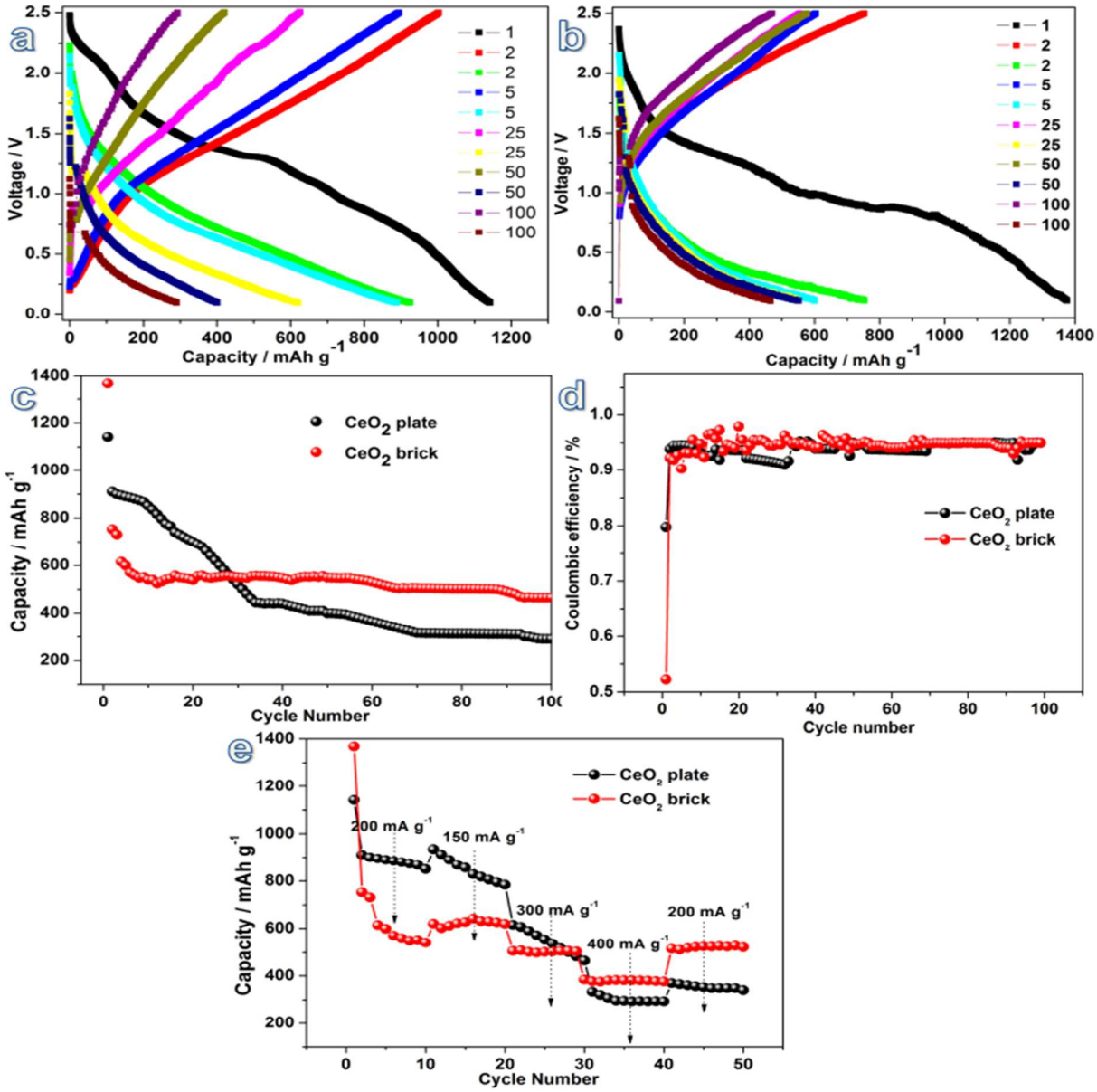

Figure 7 The discharge–charge curves (1-100 cycles) of electrodes fabricated using CeO_2 nanostructures at a current density of 200 mA g^{-1} in the voltage range of 0.1-2.5 V, a) The plate-like CeO_2 particles; b) The brick-like CeO_2 particles; c) Comparison of plate-like CeO_2 electrode and brick-like CeO_2 electrode for 100 cycles at 200 mA g^{-1}; d) Coulombic efficiency of 100 cycles at 200 mA g^{-1}, and e) Rate capability, 10 cycles were tested for each current density of the CeO_2 nanostructured electrodes.

The plate-like and brick-like CeO_2 particles were employed as lithium-ion battery anode materials. Figure 6a shows the initial discharge–charge curves of electrodes fabricated using CeO_2 nanostructures at a current density of 200 mA g^{-1} in the voltage range of 0.1-2.5 V. The brick-like CeO_2 particles electrode displayed a satisfying initial discharge capacity above 1375 mAh g^{-1}, while that of the plate-like CeO_2 particles electrode is 1100 mAh g^{-1}. The abnormally high capacity in the first discharge (far exceed the theoretical value of 623 mA h g^{-1} based on the reversible reaction) should be largely caused by the decomposition of the non-aqueous electrolyte and the formation of solid electrolyte interface (SEI) layer on the electroactive materials. The SEI layer would also partly protect the electrodes and result in relatively stable cycling

RSC Advances Accepted Manuscript

performance. [56, 57] The capacity of the brick-like CeO_2 particles electrode remains >33 % of its initial specific capacity after the subsequent 100 discharge/charge cycles, which is significantly higher than that of the plate-like electrode. It shows a remarkable decrease of the irreversible capacity loss, as shown in Figure 7a, b, in which the discharge/charge curves of these cycles overlap. 100 cycles were tested at 200 mA g^{-1} and the results from these cycles are shown in Figure 7c. It was found that the capacity of the CeO_2 particles electrodes fade immediately and then that of brick-like electrode gradually decreased to ~460 mAh g^{-1} and that of plate-like electrode is ~290 mAh g^{-1}. Despite the large irreversible loss in the first cycling, the discharge capacity is well retained during the following cycling, and the coulombic efficiency is increased to above 91% in Figure 7d, suggesting good capacity retention of two CeO_2 particles electrodes. To obtain further evidence of the high power performance of the electrodes, the rate capability was also investigated. Figure 7e shows the representative rate capability at various rates ranging from 150 mA g^{-1} to 400 mA g^{-1}. The good rate capability of the CeO_2 brick electrode is explicitly demonstrated in Figure 7e. It can be seen that the discharge capacity of CeO_2 brick electrode reaches to about 637 mAh g^{-1} after the first 10 cycles at a low rate of 150 mA g^{-1}, and then it slightly reduces to 500, and 385 mA h g^{-1} at rates of 300 mA g^{-1}, and 400 mA g^{-1}. When the current rate is returned to the initial value of 200 mA g^{-1} after 40 cycles, the electrode recovers 522 mAh g^{-1}.

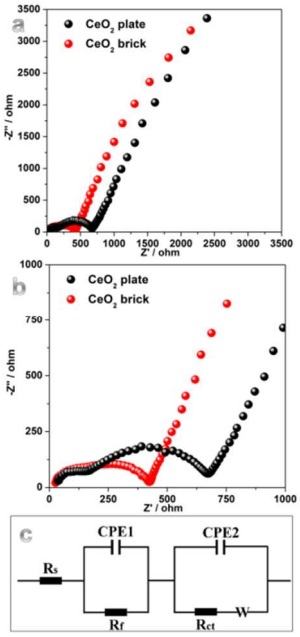

Figure 8 The electrochemical impedance spectra (EIS) of the electrodes of CeO_2 particles at room temperature, a) 0~3500 ohm, b) 0~1000 ohm, and c) The equivalent circuit for the electrochemical impedance spectrum. It consists of the electrolyte (R_s), surface film (R_f) and charge transfer (R_{ct}) resistances, constant phase elements (CPE1 and CPE2), along with the Warburg impedance (W).

Figure 8a, b shows the electrochemical impedance spectra (EIS) of the electrodes of CeO_2 particles at room temperature. In general, the impedance curves present two partially overlapped semicircles in the high- and medium-frequency regions and an inclined line in the low-frequency region. An equivalent circuit is used to fit the impedance curve is given in Figure 8c, which is similar to the circuit employed for the electrode of the lithium ion battery. [58] The semicircle can be assigned to the combination of the electrode/electrolyte interface film resistance (R_f) and the charge transfer impedance (R_{ct}), while the linear portion is designated to Warburg impedance (W), which is attributed to the diffusion of lithium ions into the bulk of the electrode materials. According to a previous report, [59, 60] the high-frequency semicircle shown in the figure is attributed to SEI film and/or contact resistance, the semicircle in the medium-frequency region is due to the charge-transfer impedance on the electrode/electrolyte interface and the inclined line corresponds to the lithium-diffusion process within the electrodes. It can be seen that the diameter of the semicircle in the medium-frequency region for the brick-like CeO_2 particles electrode electrode is much smaller than that of the plate-like CeO_2 particles electrode, indicating a lower charge-transfer resistance. The charge-transfer resistance R_{ct} was calculated to be 660 Ω (plate-like CeO_2 particles electrode) and (brick-like CeO_2 particles electrode) 418 Ω, respectively. It clearly demonstrates the reduced charge-transfer resistance of the brick-like CeO_2 particles electrode compared with that of using plate-like CeO_2 particles electrode.

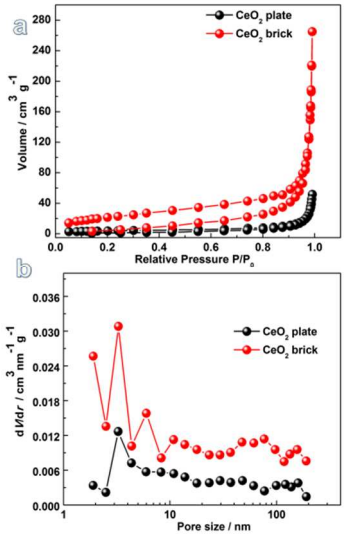

Figure 9 a) Brunauer–Emmett–Teller measurements of two mixed products (CeO_2-acetylene black-PVDF) after 100 cycles; and b) Corresponding Barrett–Joyner–Halenda pore size distribution curve.

Such a result could be ascribed to the larger surface areas accompanied by smaller particles, which facilitates the insertion of lithium ions and the access of electrolytes. [61] This enhanced kinetics is due to the fact that the BET surface area of the brick-like particle (66.7 m^2 g^{-1}) is much larger than that of the plate-like particle (8.6 m^2 g^{-1}), making the efficient contact of the brick-like particle with the electrolyte. Even after 100 cycles, the BET surface area of the CeO_2 brick particle-acetylene black-PVDF (57.2 m^2 g^{-1}) is much larger than that of the CeO_2 plate particle-acetylene black-PVDF (6.6 m^2 g^{-1}). And the pore size of mixed brick particle is ~3.2 nm, which maintains the

RSC Advances Accepted Manuscript

efficient contact of the brick-like particle with the electrolyte (Figure 9). This specific surface/interface decreases the polarization of the electrode and thus increases the charge-discharge capacity.

Conclusions

In summary, the plate-like and brick-like CeO_2 particles have been successfully prepared via a simple precursor approach. This method can be extended to using other kinds of salt precursors to prepare a series of nanostructured metal oxides by controlled thermal decomposition of the oxalate precursors. Especially, the electrochemical results showed that the electrodes containing brick-like particles exhibited an electrochemical capacity of ~460 mA h g^{-1}, and good stability up to 100 charge–discharge cycles. It is a good example to prove that physical and chemical properties of nano/microstructured materials are related to their structures, and the precise control of morphology of nanomaterials will allow us to control the performance. Exploring the electrochemical characteristics of novel nano/micromaterials may direct a new generation of Li ion battery materials.

Acknowledgements

This work is supported by the Program for New Century Excellent Talents from the Ministry of Education (**NCET**-13-0645) and National Natural Science Foundation of China (**NSFC**-21201010), the Science & Technology Foundation of Henan Province (122102210253, 13A150019), the China Postdoctoral Science Foundation (2012M521115), and the opening research foundations of State Key Laboratory of Coordination Chemistry (Nanjing University).

Notes

[a] *College of Chemistry and Chemical Engineering, Anyang Normal University, Anyang, 455000 Henan, P. R. China.*

[b] *Nanjing Xiaozhuang University, Nanjing, 211171, P. R. China*

E-mail: huanpangchem@hotmail.com; cychen@njxzc.edu.cn

[c] *State Key Laboratory of Coordination Chemistry, Nanjing University, Nanjing, 210093 Jiangsu, P. R. China.*

References

1 M. A. El-Sayed, *Acc. Chem. Res.,* 2001, 34, 257.

2 S. H. Jiao, L. F. Xu, K. Jiang and D. S. Xu, *Adv. Mater.* (Weinheim, Ger.)., 2006, **18**, 1174.

3 J. T. Zhang, Y. Tang, K. Lee and M. Ouyang, *Nature*, 2010, **466**, 91-95.

4 X. H. Zhang, Y. N. Li and C. B. Cao, *J. Mater. Chem*., 2012, **22**, 13918.

5 G. X. Zhu, Z. Xu, *J. Am. Chem. Soc*., 2011, **133**, 148-157.

6 J. F. Liu, L. L.Wang, X. M. Sun, and X. Q. Zhu, *Angew. Chem. Int. Ed.*, 2010, **49**, 3492-3495.

7 X. F. Xia, Q. L. Hao, W. Lei, W. J. Wang, D. P. Sun and X. Wang, *J. Mater. Chem.*, 2012, **22**, 16844-16850.

8 Y. Jiang, H. F. Gong, D. Volkmer, L. B. Gower and H. Cölfen, *Adv. Mater*., 2011, **23**, 3548.

9 S. Y. Gao, Z. Li, X. Jia, K. Jiang and H. Zeng, *Green Chem.*, 2010, **12**, 1442.

10 M. Han, Q. Liu, J. H. He, Y. Song, Z. Xu and J. M. Zhu. *Adv. Mater*., 2007, **19**, 1096.

11 H. Pang, Y. Y. Liu, Y. H. Ma, G. C. Li, Y. N. Ai, J. Chen, J. S. Zhang and H. H. Zheng, *Nanoscale*, 2013, **5**, 503.

12 H. B. Wu, H. Pang and X. W. Lou, *Energy Environ. Sci.*, 2013, **6**, 3619.

13 J. M. Tarascon and M. Armand, *Nature*, 2001, **414**, 359.

14 M. S. Whittingham, *Chem. Rev.*, 2004, **104**, 4271.

15 M. Okubo, E. Hosono, J. Kim, M. Enomoto, N. Kojima, T. Kudo, H. Zhou and I. Honma, *J. Am. Chem. Soc.,* 2007, **129**, 7444.

16 Y. G. Wang and Y. Y. Xia, *Adv. Mater.* 2013, **25**, 5336–5342

17 C. Z. Yuan, X. G. Zhang, L. H. Su, B. Gao and L. F. Shen, *J. Mater. Chem*., 2009, **19**, 5772-5777.

18 A. S. Arico, P. G. Bruce, B. Scrosati, J.-M. Tarascon and W. Van Schalkwijc, *Nat. Mater*., 2005, **4**, 366.

19 J. Chen and F. Y. Cheng, *Acc. Chem. Res.*, 2009, **42**, 713.

20 Y. G. Guo, J. S. Hu and L. J. Wan, *Adv. Mater.*, 2008, **20**, 2878.

21 H. Li, Z. X. Wang, L. Q. Chen and X. J. Huang, *Adv. Mater.* 2009, **21**, 4593.

22 C. Burda, X. B. Chen, R. Narayanan and M. A. El-Sayed, *Chem. Rev.* 2005, **105**, 1025.

23 G. M. Hua, L. D. Zhang, G. T. Fei and M. Fang, *J. Mater. Chem*.,2012, **22**, 6851.

24 R. J. Qi, Y. J. Zhu, G. F. Cheng and Y. H. Huang, *Nanotechnology*, 2005, **16**, 2502.

25 M. Balaguer, V. B. Vert, L. Navarrete, J. M. Serra, *Journal of Power Sources*, 2013, **223**, 214.

26 N. Izu, T. Itoh, M. Nishibori, I. Matsubara, W. Shin, *Sensors And Actuators B-Chemical*, 2012, **171**, 350.

27 D. S. Zhang, X. J. Du,L. Y. Shi and R. H. Gao, *Dalton Trans.*, 2012, **41**, 14455.

28 D. S. Zhang, F. H. Niu, T. T. Yan, L. Y. Shi, X. J. Du and J. H. Fang, *Applied Surface Science*, 2011, **257**, 10161.

29 J. Zhang, S. Ohara, M. Umetsu, T. Naka, Y. Hatakayama and T. Adschiri, *Adv. Mater*., 2007, **19**, 203.

30 H. L. Mai, D. S. Zhang, L. Y. Shi, T. T. Yan and H. R. Li, *Applied Surface Science*, 2011, **257**, 7551.

31 Z. X. Ji, X. Wang, H. Y. Zhang, S. J. Lin, H. Meng, B. B. Sun, S. J. George, T, Xia, A. E. Nel and J. I. Zink, *ACS Nano*., 2012, **6**, 5366.

32 F. F. Zhu, G. Z. Chen, S. X. Sun and X. Sun, *J. Mater. Chem. A*, 2013, **1**, 288-294.

33 N. F. Hamedani, A. R. Mahjoub, A. A. Khodadadi and Y. Mortazavi, *Sensors And Actuators B-Chemical*, 2012, **169**, 67.

34 Z. L. Zhang, D. Han, S. J. Wei and Y. X. Zhang, *Journal of Catalysis*, 2010, **276**, 16.

35 X. J. Du, D. S. Zhang, L. Y. Shi, R. H. Gao and J. P. Zhang, *J. Phys. Chem. C*, 2012, **116**, 10009.

36 S. Szenknect, A. Mesbah, D. Horlait, N. Clavier, S. Dourdain, J. Ravaux and N, Dacheux, *J. Phys. Chem. C*, 2012, **116**, 12027.

37 D. Horlait, L. Claparede, N. Clavier, S. Szenknect, N. Dacheux, J. Ravaux and R. Podor, *Inorganic Chemistry*, 2011, **50**, 7150.

38 M. A. Gabal, Shabaan A. K. Elroby and A. Y. Obaid. *Powder Technology*, 2012, **229**, 112.

39 D. E. Zhang, X. M. Ni, H. G. Zheng, X. J. Zhang, and J. M. Song. *Solid State Sciences*, 2006, **8**, 12.

40 W. Liu, L. J. Feng, C. Zhang, H. X. Yang, J. X. Guo, X. F. Liu, X. Y. Zhang and Y. Z. Yang, *J. Mater. Chem. A*, doi:10.1039/C3TA10487G.

41 H. Pang, Y. Ma, G. Li, J. Chen, J. Zhang, H. Zheng and W. Du, *Dalton Trans.*, 2012, **41**, 13284

RSC Advances Accepted Manuscript

 This journal is © The Royal Society of Chemistry 2012

42 H. Pang, J. Deng, S. Wang, S. Li, J. Du, J. Chen and J. Zhang, *RSC Advances*, 2012, **2**, 5930-5934
43 J. Y. Baek, H. W. Ha, I. Y. Kim and S. J. Hwang, *J. Phys. Chem. C*, 2009, **113**, 17392.
44 X. F. Zhou, Z. L. Hu, Y. Q. Fan, S. Chen, W. P. Ding and N. P. Xu, *J. Phys. Chem. C*, 2008, **112**, 11722.
45 S. L. Xiong, C. Z. Yuan, X. G. Zhang, B. J. Xi and Y. T. Qian, *Chemistry: A European Journal*, 2009, **15**, 5320.
46 J. C. Park, J. Kim, H. Kwon and H. Song, *Adv. Mater*., 2009, **21**, 803.
47 C. C. Hu, K. H. Chang, M. C. Lin and Y. T. Wu, *Nano Letters*, 2006, **6**, 2690.
48 X. Xia, J. Tu, X. Wang, C. Gu and X. Zhao, *J. Mater. Chem.*, 2011, **21**, 671.
49 Y. Gao, S. Chen, D. Cao, G. Wang, J. Yin, *J. Power Sources*, 2010, **195**, 1757.
50 G. V. Subba Rao, B. V. R. Chowdari, A. T. S. Wee, C. T. Lim and C. H. Sow, *Chem. Mater.*, 2008, **20**, 3360–3367.
51 H. Wang, Q. Pan, X. Wang, G. Yin and J. Zhao, *J. Appl. Electrochem.*, 2009, **39**, 1597–1602.
52 X. Li, A. Dhanabalan, K. Bechtold and C. Wang, *Electrochem. Commun*., 2010, **12**, 1222–1225.
53 C. Wang, D. Wang, Q. Wang and H. Chen, *J. Power Sources*, 2010, **195**, 7432–7437.
54 B. Varghese, M. V. Reddy, Z. Yanwu, C. S. Lit, T. C. Hoong,P. Poizot, S. Laruelle, S. Grugeon, L. Dupont and J. M. Tarascon, *Nature*, 2000, **407**, 496–499.
55 M. Sasidharan, N. Gunawardhana, M. Yoshio and K. Nakashima, *Chemistry Letters*, 2012, **4**, 386-388.
56 H. Liu, G. Wang, J. Liu , S. Qiao, H. Ahn, *J. Mater. Chem.* 2011, **21**, 3046.
57 B. Varghese, M. V. Reddy, Z. Yanwu, C. S. Lit, T. C. Hoong, G. V. Subba Rao, B. V. R. Chowdari, A. T. S. Wee, C. T. Lim, C.-H. Sow, *Chem. Mater*. 2008, **20**, 3360.
58 S. B. Yang, H. H. Song and X. H. Chen, *Electrochem. Commun*., 2006, **8**, 137-142.
59 S. Yang, H. Song and X. Chen, *Electrochem. Commun.* 2006, **8**, 137.
60 G. Wang, J. T. Bai, Y. H. Wang, Z. Y. Ren and J. B. Bai, *Scripta Materialia* 2011, **65**, 339–342.
61 X. Wang, X. Chen, L. G. Gao, H. Zheng, Z. Zhang and Y. Qian, *J. Phys. Chem.*, 2004, **108**, 16401-16404.

ToC

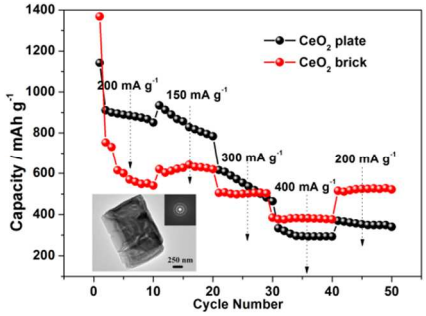

RSC Advances Accepted Manuscript